Analysis and seismic retrofit study of a heritage-listed R/C elevated water tower

S. Sorace[1] & G. Terenzi[2] & C. Mori[2]
[1]*Department of Civil Engineering and Architecture,*
University of Udine, Italy
[2]*Department of Civil and Environmental Engineering,*
University of Florence, Italy

Abstract

A heritage-listed R/C water tower designed by the world-famous Italian engineer Pier Luigi Nervi and built in the early 1930s, representative of a wide stock of heritage-listed elevated liquid storage tanks with frame staging, is examined in this study. The assessment analysis of the structure is developed with a detailed finite element model, which includes a multi spring-mass assembly to reproduce the fluid–tank dynamic interaction. The time-history evaluation enquiry shows collapse response conditions under seismic action scaled at the maximum considered earthquake (MCE) level. Based on these data, a passive supplemental energy dissipation-based retrofit hypothesis is proposed, consisting of the installation of a dissipative bracing system incorporating pressurized fluid viscous spring-dampers. The installation details the protective technology, and the benefits induced in the seismic response of the tank structure are discussed. Costs are also estimated and compared with the costs of a conventional non-dissipative bracing retrofit solution developed for the same performance.
Keywords: modern heritage structures, water storage tanks, seismic assessment, seismic retrofit, dissipative braces, fluid viscous dampers.

1 Introduction

Pre-normative R/C elevated water storage tanks are amongst the most seismically vulnerable lifelines. This is a consequence of the tall and slender geometry of staging, little redundancy and low ductility of constituting members, as well as of an unfavourable structural configuration with respect to seismic

action, i.e. with the highest portion of masses (vessel plus contained liquid) concentrated on top. Another peculiar hazard is that water towers are often situated in urban areas, sometimes in city centres, rather than in suburban areas, as normally occurs for industrial liquid tanks. Therefore, their partial or global failure can cause heavy damage to the surrounding buildings and infrastructures, with serious consequences for the safety of a great number of inhabitants [1].

At the same time, several old water towers are now considered historically significant and have been included in the heritage listings of several earthquake-prone countries. This imposes their preservation and possible seismic retrofit by means of low impact structural solutions, respectful of their recognised architectural and engineering value.

In view of this, the class of advanced earthquake protection technologies based on the concept of supplemental energy dissipation [2] can offer effective rehabilitation solutions for these special structures too, in addition to their successful application to frame buildings. Hence, a research programme aimed at extending to this field the use of dissipative bracing systems, deeply enquired by the first two authors for various types of building structures, was recently undertaken. A first representative case study, represented by an R/C frame-supported elevated tank built in the early 1930s as a water supply for Santa Maria Novella Station in Florence, still in service, is examined herein. A photographic view of the tower showing its appearance in 1935, a few months after the completion of the construction works, is displayed in Figure 1(a).
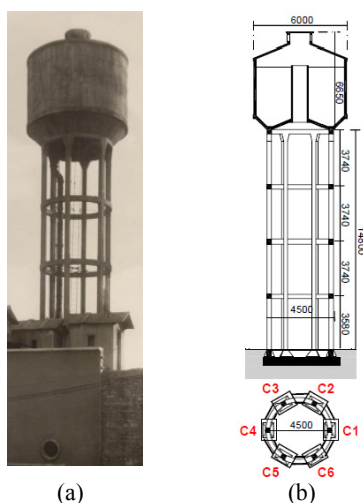

(a) (b)

Figure 1:   (a) View of the water tower taken in 1935; (b) vertical section and base plan.

The R/C structure was designed by the world-famous Italian engineer Pier Luigi Nervi, and offered noticeable innovations as compared to the recurrent geometrical and structural characteristics of R/C frame elevated tanks at the time. These innovative features consist of small-sized columns and ring beams,

obtained by using high-strength concrete and increased quantities of reinforcing steel bars and stirrups, as well as of a more accentuated vertical layout of columns, and of the absence of bracings and intermediate slabs within the frame skeleton. Indeed, more massive member sections, pronounced flaring layouts in the bottom portions of the staging, slabs at various staging levels along the height and continuous curtains of R/C braces are typical of frame tanks built from 1900s to 1930s. The vessel of the tank in Santa Maria Novella Station was rather innovative too, being among the earliest Intze-type realizations in Italy, constituted by two thin coaxial R/C cylindrical walls, the inner of which houses a manhole. The vessel is completed by an external inverted truncated cone and an internal conical floor slab, bottom and top ring beams, a conical roof slab, and a cylindrical lantern on top for aeration and natural illumination.

The cross section and base plan, derived from the original design documentation collected through record research, are illustrated in Figure 1(b). The structure is 21.45 m high, with staging height of 14.8 m (3.58 m being the height of the first staging level, and 3.74 m the height of the second through fourth levels), and vessel height of 6.65 m. The maximum available water volume is 100 m^3. The internal diameters of the vessel and coaxial cylindrical manhole are equal to 6 m and 1 m, respectively; the external diameter of the staging base is equal to 4.5 m. The external wall, manhole wall, bottom slab and floor slab of the vessel are 140 mm, 80 mm, 150 mm and 90 mm thick, respectively. The R/C frame structure is constituted by six columns with mutual section of (300×300) mm×mm (column alignments are numbered in the plan of Fig. 3 with symbols C1 through C6); three intermediate ring beams with section of (300×300) mm×mm, situated at a mutual distance along the height of about 3.7 m; and a top ring beam sized (300×500) mm×mm, also constituting the annular support of the vessel. The foundation consists of six plinths under the columns with base section of (1400×1100) mm×mm and a connecting ring beam with rectangular section of (450×650) mm×mm. These members lie on a several-meter-deep compressed mixed mortar–stone substrate, specially built to significantly increase the soil bearing capacity and prevent any ground settlement under the design static loads, according to a typical building protocol used for elevated tanks at the time.

The mechanical properties of concrete and steel and reinforcement details have also been drawn from the original design drawings and characterization test reports. These documents highlight that the compressive cube strength of concrete, $f_{c,cube}$, is not less than 40 MPa for the vessel and supporting structures, and 30 MPa for the foundation members. Reinforcing steel is in smooth bars with a minimum yield stress, $f_{y,min}$, equal to 220 MPa.

2 Finite element model of the water tower

The finite element model of the water tower structure was generated by SAP2000NL calculus program [3]. A perspective view of the model is displayed in Figure 2(a), where the global reference coordinate system, constituted by the Cartesian axes x, y and z, is visualised too.
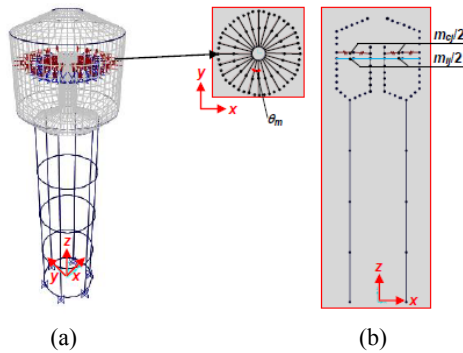
Figure 2: Perspective view, plan and vertical cross section of the finite element model.

The computational simulation of fluid–tank interaction was carried out according to the classical Housner's two-mass equivalent model [4], which is being widely used in most international Seismic Standards and Design Guidelines on liquid storage tanks [5–7]. The model is sketched for a cylindrical tank without coaxial manhole in Figure 3(a), where m_i is the impulsive mass, corresponding to the fraction of liquid volume situated in the lower region of the tank, which oscillates in unison with it, thus acting like a mass rigidly connected to the tank wall; m_c the convective mass, corresponding to the remaining fraction of liquid volume, situated in the upper region of the tank, which undergoes sloshing motion; h_i', h_c' the heights of the two masses from the bottom of the tank wall, equal to the heights of the resultants of the impulsive and convective pressure distributions on the wall and the base, in the general case of non-horizontal floor surface (as for the vessel of the case study tank); h_L the liquid height; D the tank diameter; and $k_c/2$ the stiffness of each one of the two identical elastic springs connecting m_c to the tank wall (m_i is rigidly connected to it, for the observations above).
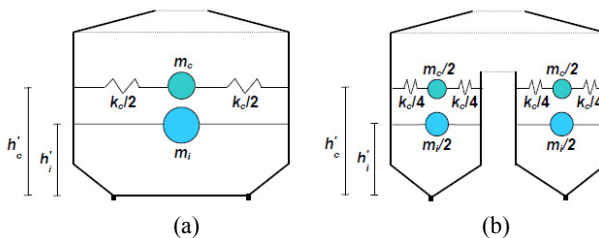

Figure 3: Reference parameters of Housner's two-mass model.

This model yields a reliable idealization of the phenomenon also in the presence of coaxial walls, provided that the inner volume is a relatively small portion of the total tank volume. This condition is normally met by all types of elevated vessels with inner manholes, as is the case of the examined tank, where the volume of the manhole space is only a rounded 2.5% of the total volume up

to the water free surface. In order to geometrically reproduce the inner wall in the finite element model, m_c and m_i were firstly split in two identical portions, with masses equal to $m_c/2$, $m_i/2$, and convective mass spring stiffness $k_c/4$ for each spring, as illustrated in the generalized two-mass model scheme sketched in Figure 3(b). Secondly, a 3-D implementation of the basic 2-D layout of the two-mass model was adopted, so that the hydrodynamic pressure effects are properly spread across the circumference of the vessel walls. This was obtained by subdividing the water volume into n equal fractions, each one being identified in plan with a circumferential angle θ_n equal to $180°/n$, which determines m_{cj} convective and m_{ij} impulsive masses, and k_{cj} convective mass spring stiffness of the j-th volume fraction equal to $m_{cj}=m_c/n$, $m_{ij}=m_i/n$ and $k_{cj}=k_c/n$ ($j=1,\ldots,n$). Then, m_{cj}, m_{ij} and k_{cj} were split in the two sub-portions of each volume fraction consistently with Figure 3(b) scheme. The parameters relevant to each sub-portion, i.e. $m_{cj}/2$ for the two split convective masses, $m_{ij}/2$ for the two split impulsive masses, and $k_{cj}/4$ for the four convective mass springs, are visualized in the plan and vertical cross sections of the finite element model shown in Figure 2(b). The influence of n on the finite element model response was evaluated by varying it from 6 (i.e. $\theta_n=30°$) to 18 ($\theta_n=10°$). The segmental reproduction of the analytical hydrodynamic pressure distribution on the vessel walls provided by the 3-D implementation of the two-mass model was acceptable in all cases and totally satisfactory starting from $n=12$. The results of modal and time-history analyses are presented in the following for this n value, to which $\theta_n=15°$ corresponds. The m_i, m_c, $h_i^{'}$, $h_c^{'}$ and k_c values assumed in the analysis were computed by means of the following normative expressions for circular tanks [5–7], derived with slight modifications from the original two-mass model analytical formulation [4]:

$$\frac{m_i}{m_L} = \frac{\tanh\left(0.866\dfrac{D}{h_L}\right)}{0.866\dfrac{D}{h_L}} \tag{1}$$

$$\frac{m_c}{m_L} = 0.23\frac{\tanh\left(3.68\dfrac{h_L}{D}\right)}{\dfrac{h_L}{D}} \tag{2}$$

$$\frac{h_i^{'}}{h_L} = 0.45 \qquad \text{for } \frac{D}{h_L} < 0.75 \tag{3a}$$

$$\frac{h_i^{'}}{h_L} = \frac{0.866\dfrac{D}{h_L}}{2\tanh\left(0.866\dfrac{D}{h_L}\right)} - 0.125 \qquad \text{for } \frac{D}{h_L} \geq 0.75 \tag{3b}$$

$$\frac{h_c^{'}}{h_L} = 1 - \frac{\cosh\left(3.68\frac{h_L}{D}\right) - 2.01}{3.68\frac{h_L}{D} \cdot \sinh\left(3.68\frac{h_L}{D}\right)} \tag{4}$$

$$k_c = 3.68\frac{m_c \cdot g}{D}\tanh\left(3.68\frac{h_L}{D}\right) \tag{5}$$

where $m_L = m_i + m_c$ is the total liquid mass, and g is the acceleration of gravity. In order to consider the presence of the manhole, calculation of parameters m_c, m_i, k_c, $h_i^{'}$ and $h_c^{'}$ was carried out by referring to a reduced D diameter, instead of 6 m, to obtain the same maximum water volume of 100 m³ as the equivalent circular tank without inner wall. Based on a liquid height h_L of 3.9 m, the reduced D value results to be equal to 5.71 m. The m_i, m_c, $h_i^{'}$, $h_c^{'}$ and k_c values calculated for h_L and D are as follows: m_i=66,770 kN·s²/m, m_c=33,230 kN·s²/m, $h_i^{'}$=2.38 m, $h_c^{'}$=2.84 m and k_c=197 kN/m, from which m_{ij}=m_i/12=5564 kN·s²/m, m_{cj}=m_c/12=2770 kN·s²/m, k_{cj}=k_c/12=16.4 kN/m, for each water volume fraction, and m_{ij}/2=2782 kN·s²/m, m_{cj}/2=1385 kN·s²/m, k_{cj}/4=4.1 kN/m, for the left and right portions of each volume fraction, are obtained for the 3-D implemented finite element model parameters, for n=12. These data were introduced as input in the modal and time-history analyses of the structure, presented in the next sections.

3   Performance assessment analysis in current conditions

A modal analysis was initially carried out by the finite element model described above, which shows pairs of identical horizontal translational modes along the two axes in plan, x and y, as a consequence of the axial symmetry of the structure with respect to the vertical direction z. The first pair of modes, purely translational in x and y, is determined by the convective water masses, with vibration period of 2.58 s and effective modal mass (EMM) equal to 21.9% along both axes. The second pair (translational too), is related to the impulsive water masses plus the masses of the tank structure, with vibration period of 1.29 s and EMM equal to 70.4%. The first and second mode pairs are sufficient to activate a summed effective modal mass (SEMM) greater than 90% (namely 92.3%) of the total seismic mass of the tank, along x and y. The first and second vertical translational modes have periods of 0.05 s and 0.02 s, and EMMs of 88.6% and 2.1%, respectively, with SEMM of 90.7%. The first and second rotational modes around the vertical axis z have periods of 0.9 s and 0.01 s, with EMMs of 92.4% and 4.1%, and SEMM of 96.5%. 80 modes are needed to activate about 100% of seismic masses along and around all axes.

The performance evaluation enquiry was carried out for the four reference seismic levels fixed in the Italian Standards [8], that is, Frequent Design Earthquake (FDE, with 81% probability of being exceeded over the reference time period V_R); Serviceability Design Earthquake (SDE, with 50%/V_R

probability); Basic Design Earthquake (BDE, with 10%/V_R probability); and Maximum Considered Earthquake (MCE, with 5%/V_R probability). The V_R period is fixed at 75 years, which is obtained by multiplying the nominal structural life V_N of 50 years by a coefficient of use c_u equal to 1.5, imposed to structures whose seismic resistance is of importance in view of the consequences associated with their possible collapse. By referring to topographic category T1 (flat surface), and C-type soil (deep deposits of dense or medium-dense sand, gravel or stiff clay from several ten to several hundred meters thick), the resulting peak ground accelerations for the four seismic levels referred to the city of Florence are as follows: 0.082 g (FDE), 0.098 g (SDE), 0.223 g (BDE), and 0.27 g (MCE), for the horizontal motion components; and 0.017 g (FDE), 0.022 g (SDE), 0.079 g (BDE), and 0.111 g (MCE), for the vertical component. The time-history analyses were developed by assuming artificial ground motions as inputs, generated in families of seven from the spectra above, both for the horizontal components (two families) and the vertical one (one family). As required by the Italian Standards, as well as by several other international seismic Codes and Regulations, in each time-history analysis the accelerograms were applied in groups of three simultaneous components, i.e. two horizontal components, with the first one selected from the first generated family of seven motions, and the second one selected from the second family, plus the vertical component.

At a first step of the assessment enquiry, the staging members were modelled as elastic elements. The results of the analyses at FDE and SDE levels show safe response conditions of columns and beams, with maximum values of the inter-level drift ratio (i.e. the ratio of inter-level drift to inter-level staging height) ranging from 0.2% on the first level to 0.26% on the third level (FDE), and from 0.24% to 0.32% (SDE). These values are below the 0.33% limitation adopted by [8] at the Operational (OP) performance level for frame structures interacting with drift-sensitive non-structural elements. The resulting FDE-OP and SDE–OP correlations assess a satisfactory performance, ensuring adequate protection to the vertical water pipes and the electrical equipment of the auxiliary pumping plant, which are the only non-structural elements housed in this structure. The time-history response to the input motions scaled at the BDE and MCE levels highlight that bending-compression verifications are not passed by 50% (BDE) and 90% (MCE) of columns, and shear verifications by 60% (BDE) and 85% (MCE) of beams.

In view of this very high stress demand, a second step of the time-history assessment enquiry was developed at the BDE and MCE levels, where the plastic behaviour of beams and columns was investigated by incorporating lumped plastic hinges at the end sections of these members. The non-linear response of the hinges is governed by a bilinear skeleton curve, built by assigning the yielding and ultimate values of the resisting moments, M_y and M_u, and chord rotations, θ_y and θ_u, of the member end sections. In particular, the two chord rotations were computed by expressions (8.7.2.1a) and (C8A.6.1) provided by the Commentary to the Italian Technical Standards [9], not reported here for brevity's sake. Since the response of the plastic hinge elements is expressed in

terms of plastic chord rotation, θ_{pl}, rather than total (elastic plus plastic) rotation, the response capacity of columns and beams was evaluated by comparison with the ultimate value of θ_{pl}, $\theta_{pl,u}$, obtained by subtracting θ_y from θ_u. For columns, $\theta_{pl,u}$=0.406×10^{-2} radians is computed for the base sections on the first level, with N_s=330 kN, as mentioned above.

The analyses carried out with the input motions scaled at the BDE level highlight plastic rotations in 12 out of 24 columns, with maximum θ_{pl} values equal to 0.267×10^{-2} radians, attained in the first level base sections. Furthermore, shear verifications are not met by 60% of beams. These data assess severely damaged response conditions, but with some residual margins towards structural collapse, which allows meeting the basic requirement of the Collapse Prevention (CP) performance level. The results of the analyses at the MCE show that the numerical collapse of the six columns on the first level, and thus of the model, is reached for all seven groups of input ground motions. As way of example of the pre-collapse hysteretic response obtained, the bending moment-plastic rotation response cycles in the base section of a first level column (number C2 in the plan section of Figure 1) and the maximum inter-level drift ratios induced by the most severe among the seven groups of input motions are plotted in Figure 4.
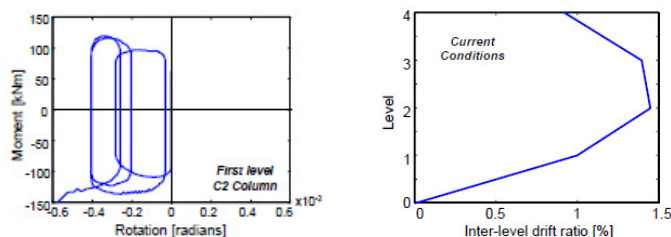

Figure 4: Response cycles of the base plastic hinge of first-level C2 column and maximum inter-level drift ratio profile in pre-collapse conditions.

The hysteretic cycles show a divergence of the numerical solution starting from a θ_{pl} value equal to about 0.55×10^{-2} radians, included within the $\theta_{pl,lim,CP}$ range above, after three complete response cycles, the widest of which is characterized by a maximum θ_{pl} value of about 0.4×10^{-2} radians, i.e. approximately equal to $\theta_{pl,u}$. Similar results are observed for the base and top sections of all other first level columns. The drift ratio profile highlights pre-collapse values of 1.08%, 1.4%, 1.46%, and 1.02% at the first through fourth level. The maximum base shear computed in pre-collapse response conditions is equal to 407 kN.

The response of the vessel structure results to be safe up to the MCE, highlighting the need for seismic rehabilitation limited to the staging portion of the tank. This is also confirmed by the verifications on the foundation, met both by the plinths and the connecting ring beams. Furthermore, the stress states transferred by the foundation to the hard substrate are always compressive, with

no risk of overturning for the tank, reaching peak local values far from the estimated ultimate bearing capacity of the substrate.

4 Dissipative bracing retrofit solution

Fluid viscous (FV) dampers are among the most widely used types of devices installed in dissipative bracing technologies worldwide. This is owed to their high damping capacities, stable mechanical properties over time, simple installation procedures, competitive costs and, in the case of pressurized elements, inherent self-centering qualities [10]. Within this class, a special system incorporating pressurized FV devices has been studied for several years by the first two authors, focusing attention on its application to frame buildings [11–15]. A new research study was recently started to extend the use of the system to the seismic retrofit of elevated tanks with frame staging, as discussed herein. A typical cross section of a FV spring-damper mounted in the fluid viscous dissipative bracing system is illustrated in Figure 5(a).

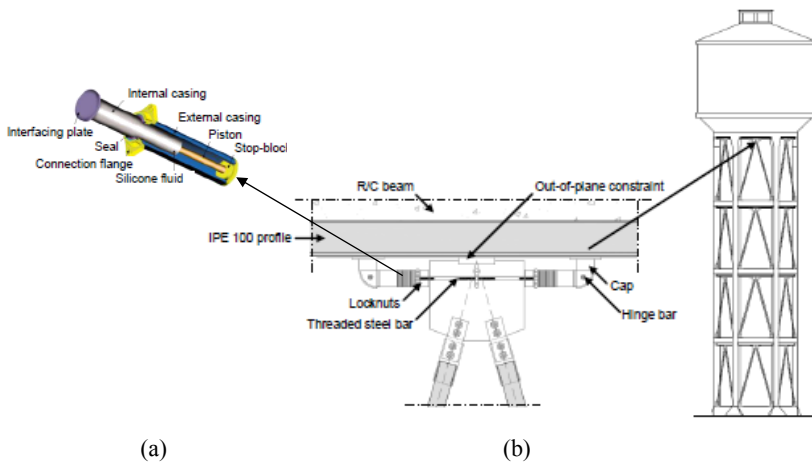(a)   (b)

Figure 5:   Cross section of a FV spring-damper and installation details of the dissipative bracing system.

The time-dependent F_d damping and F_{ne} non-linear elastic reaction forces corresponding to the damper and spring functions are effectively simulated by the following analytical expressions [10]:

$$F_d(t) = c\,\mathrm{sgn}(\dot{x}(t))|\dot{x}(t)|^{\alpha} \qquad (6)$$

$$F_{ne}(t) = k_2 x(t) + \frac{(k_1 - k_2)x(t)}{\left[1 + \left|\dfrac{k_1 x(t)}{F_0}\right|^5\right]^{1/5}} \qquad (7)$$

where t=time variable; c=damping coefficient; sgn($\cdot$)=signum function; $\dot{x}(t)$=device velocity; $|\cdot|$=absolute value; α=fractional exponent, ranging from

0.1 to 0.2 [10]; F_0=static pre-load force; k_1, k_2=stiffness of the response branches situated below and beyond F_0; and $x(t)$=device displacement.

The installation layout of the FV springs-dampers is identical to the basic configuration devised for frame buildings [11–15], where a pair of interfaced devices is mounted in parallel with the relevant beam axis, at the tip of each couple of supporting steel braces (Figure 5(b)). Consistently with the axial symmetry of the staging structure, the dissipaters are installed in all bays, as well as on all levels, which determines a total of 48 (24 pairs) dissipaters. The design of the system was developed by assigning a fraction of 80% of total seismic input energy of the protected structure to the set of incorporated devices. In order to unify the connecting steel plates of the device pairs and standardize relevant installation works, a single spring-damper type was adopted at all levels of the staging structure, whose damping capacity was selected from the manufacturer's basic catalogue [16] so as to meet the 80% energy fraction demand above. This was obtained by installing one of the smallest PFV device types in current production, characterised by the following values of the mechanical parameters included in Eqs. (6) and (7): c=2.94 kN·(s/mm)$^\alpha$; α=0.2; k_2=0.91 kN/mm; k_1=15 k_2; and F_0=5 kN. Further mechanical properties are: nominal energy dissipation capacity E_n=1.5 kJ; stroke d_{max}=±20 mm; and maximum reaction force R_{max}=±30 kN. Based on the R_{max} value, tubular profiles sized 48.3 mm (diameter)×3.2 mm (thickness) are adopted as supporting steel trusses.

A new modal analysis carried out by this model shows a first pair of translational modes in x and y associated to the convective water masses, like for the original tank. The vibration period is coincident (2.58 s), whereas the effective modal mass is slightly reduced (19.2% instead of 21.9%), owing to the increase of the frame staging masses determined by the incorporation of the steel members constituting the dissipative bracing system. The second pair of modes is related to the impulsive water masses plus the masses of the tank structure in protected configuration too, with vibration period of 1.03 s and EMM equal to 73.9%, yielding a SEMM of the first and second horizontal translational mode pairs equal to 92.8%. The first and second vertical translational modes have periods of 0.04 s and 0.015 s, and EMMs of 91.2% and 1.8%, respectively, with SEMM of 93%. The first and second rotational modes around z have periods of 0.72 s and 0.01 s, with EMMs of 93.7% and 3.2%, and SEMM of 96.9%. 43 modes are needed in this case to activate about 100% of seismic masses along and around the three axes.

The results of the time-history verification analyses in rehabilitated conditions show that the response of columns becomes totally elastic. At the same time, all beams meet shear verifications. The maximum base shear is equal to 326 kN, with 20% reduction as compared to the response in current conditions. Remarkable benefits are obtained also in terms of maximum inter-level drift ratio, which is constrained within 0.4% (Figure 6), i.e. below the 0.5% drift limitation assumed in [8] for R/C frame structures at the Immediate Occupancy performance level. As highlighted by the diagram in Figure 6, the damping action of the FV-DB system also determines a more uniform drift profile along the height, with maximum 20% differences among the peak drifts

on the four levels, as compared to about 40% differences surveyed in current configuration.
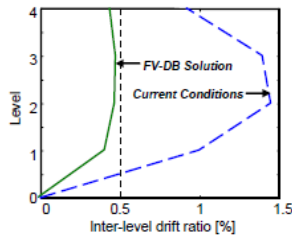

Figure 6:   Maximum inter-level drift ratio profile in retrofitted conditions.

The response of the FV dissipaters is visualized by the total reaction force–displacement $[(F_d(t)+F_{ne}(t))–x(t)]$ cycles of the pair of devices situated at the second level of the staging structure – where the maximum inter-level drifts are surveyed – in the bay enclosed between the reference columns C1 and C2, plotted in Figure 7(a). The cycles exhibit peak displacements equal to about 10.5 mm, far below the available stroke limit of ±20 mm mentioned above. The energy time-histories of the structure in x direction (practically coinciding with the response histories in all directions in plan, due to the axial symmetry of the structure) are graphed in Figure 7 too, showing that about 80% of the total input energy is actually absorbed by the whole set of dissipaters, as targeted in the system design.
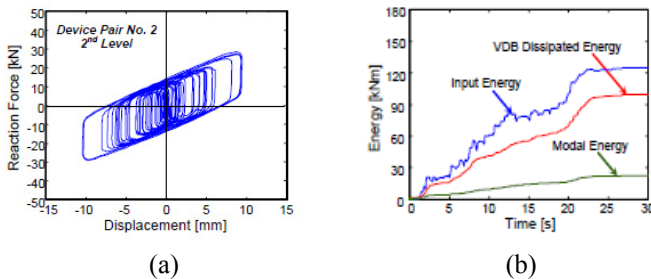

| (a) | (b) |

Figure 7:   Response cycles of a FV device pair situated at the second level and energy time-histories in x direction.

FDE, SDE and BDE-related performance too, not detailed here for brevity's sake, results to be significantly improved by the retrofit intervention. This is assessed by peak inter-level drift ratios reduced by about 55% at FDE and SDE, as compared to current conditions, and equal to 0.31% at BDE, which allows meeting the 0.33% limitation relevant to the OP level for this earthquake level too, in addition to FDE and SDE.

The estimated cost of the retrofit intervention amounts to about 60,000 Euros, installation works included, 32,000 Euros being the cost of the spring-dampers, and 28,000 Euros of the steel trusses and connecting plates. This cost is about

half the one of alternative traditional retrofit interventions designed for the same performance, which also result to be much more intrusive, both from a structural and an architectural viewpoint.

Acknowledgement

References

[1] Rai, DC. Elevated tanks. In Jain, Lettis, Bardet and Murty (Eds.). 2001 Bhuj, India earthquake reconnaissance report. Earthquake Spectra, Supplement A to 18, pp. 279–295, 2002.

[2] Christopoulos, C and Filiatrault, A. Principles of passive supplemental damping and seismic isolation. IUSS Press, Pavia, Italy: 2006.

[3] Computers and Structures Inc. Sap2000nl. Structural Analysis Programs – Theoretical and Users Manual. Version No. 17.01, CSI, Berkeley, CA, 2014.

[4] Housner, GW. Dynamic behavior of water tanks. Bulletin of the Seismological Society of America, 53, pp. 381–387, 1963.

[5] ACI 350.3-06. Seismic design of liquid-containing concrete structures. ACI – American Concrete Institute, Farmington Hills, MI (USA), 2006.

[6] IITK-GSDMA. Guidelines for seismic design of liquid storage tanks. National Information Center of Earthquake Engineering, Kanpur, India, 2007.

[7] EN 1998-4. Eurocode 8: Design of structures for earthquake resistance – Part 4: Silos, tanks and pipelines. ECS – European Committee for Standards, Brussels, Belgium, 2006.

[8] Nuove Norme Tecniche per le costruzioni [in Italian]. G.U., Rome, Italy, 2008.

[9] Commentary on the Technical Standards on Constructions [in Italian]. G.U., Rome, Italy, 2009.

[10] Sorace, S. and Terenzi, G. Non-linear dynamic modelling and design procedure of FV spring-dampers for base isolation. Engineering Structures, 23, pp. 1556–1567, 2001.

[11] Sorace, S. and Terenzi, G. Seismic protection of frame structures by fluid viscous damped braces. Journal of Structural Engineering, ASCE, 134, pp. 45–55, 2008.

[12] Sorace, S. and Terenzi, G. Fluid viscous damper-based seismic retrofit strategies of steel structures: General concepts and design application. Advanced Steel Construction, 5, pp. 322–339, 2009.

[13] Sorace, S., Terenzi, G. and Fadi, F. Shaking table and numerical seismic performance evaluation of a fluid viscous-dissipative bracing system. Earthquake Spectra, 28, pp. 1619–1642, 2012.

[14] Sorace, S. and Terenzi, G. Dissipative bracing-based seismic retrofit of R/C school buildings. The Open Construction & Building Technology Journal, 6, pp. 334–345, 2012.

[15] Sorace, S and Terenzi, G. Motion control-based seismic retrofit solutions for a R/C school building designed with earlier Technical Standards. Bulletin of Earthquake Engineering, 12, pp. 2723–2744, 2014.

[16] Jarret SL. "Shock-Control Technologies", http://www.introini.info, 2013.